Relaxation mechanisms in a disordered system with Poisson-level statistics

Janez Bonča[1,2] and Marcin Mierzejewski[3]

[1]*Department of Physics, Faculty of Mathematics and Physics, University of Ljubljana, 1000 Ljubljana, Slovenia*
[2]*Department of Theoretical Physics, J. Stefan Institute, 1000 Ljubljana, Slovenia*
[3]*Department of Theoretical Physics, Faculty of Fundamental Problems of Technology, Wrocław University of Science and Technology, 50-370 Wrocław, Poland*

(Received 3 December 2021; revised 3 March 2022; accepted 7 April 2022; published 22 April 2022)

We discuss the interplay between many-body localization and spin symmetry. To this end, we study the time evolution of several observables in the anisotropic t-J model. Like the Hubbard chain, the studied model contains charge and spin degrees of freedom, yet it has smaller Hilbert space and thus allows for numerical studies of larger systems. We compare the field disorder that breaks the $\mathbb{Z}_2$ spin symmetry and a potential disorder that preserves the latter symmetry. In the former case, sufficiently strong disorder leads to localization of all studied observables, at least for the studied system sizes. However, in the case of symmetry-preserving disorder, we observe that odd operators under the $\mathbb{Z}_2$ spin transformation relax towards the equilibrium value at relatively short timescales that grow only polynomially with the disorder strength. On the other hand, the dynamics of even operators and the level statistics within each symmetry sector are consistent with localization. Our results indicate that localization exists within each symmetry sector for symmetry-preserving disorder. Odd operators' apparent relaxation is due to their time evolution between distinct symmetry sectors.

DOI: 10.1103/PhysRevB.105.155146

I. INTRODUCTION

The many-body localization (MBL) [1–4] phenomenon has been most frequently studied in one-dimensional (1D) disordered systems with either charge or spin degrees of freedom [5–16]. Even though research in this field mainly focused on a few of the simplest prototype model Hamiltonians for MBL such as the disordered XXZ model, the type of the transition and even the existence of the MBL phase in the thermodynamic limit are still under intense consideration [17–27]. One of the specific open problems is the effect of various symmetries on the existence of MBL phase [28,29]. There are reports that non-Abelian symmetry precludes MBL [28,30,31], while other investigations claim that the non-Abelian symmetry is protected by MBL [32].

Shifting the focus to more complex prototype models that contain charge and spin degrees of freedom, such as the 1D Hubbard model with potential disorder, the existence of the full MBL phase is even more elusive. In Refs. [33–36] the authors investigated the time evolution of spin and charge imbalance as well as transport properties in the Hubbard model. Their results are consistent with localized/nonergodic charge degrees of freedom, while due to the preserved SU(2) symmetry the spin degrees of freedom remain delocalized/ergodic up to extremely large values of potential disorder. Similar conclusions were drawn based on the statistics of adjacent energy levels [37] and by counting the maximal number of local integrals of motion [38]. Subdiffusive time evolution of charge particles was found in the related t-J model [39] with potential disorder.

The effect of symmetry-preserving disorder was addressed already in noninteracting one-dimensional random hopping systems. In the case of systems with chiral or sublattice symmetry where particles can hop only between even and odd lattice sites, there is a diverging mean density of states at zero energy [40–42], which can lead to the delocalization transition [43–46].

The main goal of this paper is to compare the effects of spin-symmetry-preserving and symmetry-breaking disorders on the dynamics of charge and spin degrees of freedom. In the case of potential disorder, the behavior of specific spin degrees of freedom is inconsistent with the full MBL state due to the $\mathbb{Z}_2$ spin symmetry. This observation is based on relatively fast relaxation of spin observables that are odd under the later $\mathbb{Z}_2$ spin transformation; that is, the only nonzero matrix elements of these operators connect two distinct symmetry sectors. While this observation seems to preclude the MBL state, the statistics of adjacent energy levels computed within each symmetry sector at large potential disorder approaches Poisson statistics.

We have organized this paper as follows: in Sec. II, we present the model and the numerical method; we also discuss how the symmetry properties of the model depend on the type of disorder. Next, we present the time evolution of the charge and spin imbalance and present a simplified model that explains the unusual relaxation of the spin imbalance in the presence of the potential disorder. We further present time evolutions of various charge and spin correlation functions, followed by an analysis of charge and spin entanglement entropies. Based on the spectral level statistics, we discuss the

apparent inconsistency between the relaxation of the spin imbalance and the Poisson level statistics, both observed under the influence of strong potential disorder.

II. MODEL AND METHOD

We investigate the anisotropic t-J model on a one-dimensional ring with L sites and $N_f = L/2$ fermions in the total $S^z = 0$ subspace in the presence of either a random external magnetic field $h_i \in [-2W_s, 2W_s]$ or random potential $\epsilon_i \in [-W_c, W_c]$,

$$H = -t_0 \sum_{i,\sigma} c^\dagger_{i,\sigma} c_{i+1,\sigma} + \text{c.c.} + J_z \sum_i S^z_i S^z_{i+1} - n_i n_{i+1}/4 + \frac{J_\perp}{2} \sum_i S^+_i S^-_{i+1} + S^-_i S^+_{i+1} + \sum_i h_i S^z_i + \epsilon_i n_i. \quad (1)$$

The fermion operators $c_{i,\sigma}$ and $n_i = \sum_\sigma c^\dagger_{i,\sigma} c_{i,\sigma}$, as well as the spin operators $S^{\pm,z}_i$, act in the Hilbert space spanned locally by only three states, $|0\rangle_i$, $|\uparrow\rangle_i$, and $|\downarrow\rangle_i$. The absence of doubly occupied states $|\uparrow\downarrow\rangle_i$ in the t-J model allows studying charge and spin dynamics for much larger systems than would be possible for the Hubbard chain. This property is the main motivation for the choice of Hamiltonian. We perform multiple time evolutions based on the Lanczos technique, with each evolution starting from a different set of either random h_i or ϵ_i. The main goal of this work is to compare the time evolution of spin and charge degrees of freedom under the influence of two different types of disorder. For this reason we choose, following Ref. [37], the initial state that possesses a charge-density-wave order as well as a staggered spin orientation configuration $|\Psi_0\rangle$, defined as

$$|\Psi_0\rangle = |\uparrow 0 \downarrow 0 \uparrow 0 \downarrow 0 \ldots\rangle, \quad (2)$$

$$|\bar{\Psi}_0\rangle = \hat{U}|\Psi_0\rangle = |\downarrow 0 \uparrow 0 \downarrow 0 \uparrow 0 \ldots\rangle, \quad (3)$$

where $|\bar{\Psi}_0\rangle$ represents a state with globally reversed spin projections S^z_i via the unitary transformation $\hat{U} = \prod_i (1 - n_i + S^+_i + S^-_i)$. In addition, we compute the level statistics of the energy spectra. We typically take $N_r = 500$–1500 realizations of the disorder. We measure time in units of $[1/t_0]$ and set $t_0 = J_z = 1$ and $J_\perp = 1.5$.

There exists a significant difference between the two systems under the influence of potential ($W_c \neq 0, W_s = 0$) and field ($W_s \neq 0, W_c = 0$) disorders. Since we have set $J_z \neq J_\perp$, the SU(2) symmetry is broken even at $W_{c(s)} = 0$. In the case of the potential disorder and for $S^z_{\text{tot}} = 0$, the Hamiltonian remains invariant under the $\mathbb{Z}_2$ spin transformation $\hat{U}$, which is closely related to the global π rotation around the x axis [47]. Since $\hat{U}\hat{U} = \hat{U}\hat{U}^\dagger = 1$, each eigenstate consists of either a symmetric combination of states ($\hat{U}|\Psi_S\rangle = |\Psi_S\rangle$) or an antisymmetric combination of states ($\hat{U}|\Psi_A\rangle = -|\Psi_A\rangle$), which differ by a global reversal of S^z_i, $|\Psi_{S/A}\rangle = (|\Psi\rangle \pm \hat{U}|\Psi\rangle)/2$. The Hamiltonian thus separates into two blocks with equal numbers of symmetric and antisymmetric functions.

III. CHARGE AND SPIN IMBALANCE

We start by presenting the time propagation of the charge and spin imbalance as defined by the following operators:

$$\hat{P}_c = \frac{1}{N_f} \sum_{i=1}^{L} (-1)^{i+1} n_i, \quad (4)$$

$$\hat{P}_s = \frac{2}{N_f} \sum_{i=1}^{L} (-1)^{\sum_{j=1}^{i-1} n_j} S^z_i. \quad (5)$$

The initial state is chosen such that $\hat{P}_{c(s)}|\Psi_0\rangle = |\Psi_0\rangle$. Note also that $\hat{P}_s$ is odd under the $\mathbb{Z}_2$ spin transformation, $\hat{U}\hat{P}_s\hat{U} = -\hat{P}_s$; thus, it connects the symmetric and antisymmetric sectors, while its matrix elements within each symmetry block vanish, $\langle\Psi_S|\hat{P}_s|\Phi_S\rangle = \langle\Psi_A|\hat{P}_s|\Phi_A\rangle = 0$. Consequently, in the basis of the eigenstates of the Hamiltonian, $\hat{P}_s$ has no diagonal matrix elements. In contrast $\hat{P}_c$ is even, $\hat{U}\hat{P}_c\hat{U} = \hat{P}_c$, and $\langle\Psi_S|\hat{P}_c|\Phi_A\rangle = 0$.

We first show the charge imbalance, presented in Fig. 1(a), $P_c(t) = \langle\hat{P}_c\rangle_t$, where $\langle\cdots\rangle_t$ indicates multiple time evolutions from the initial $|\psi_0\rangle$, averaged over different random realizations of either potential or magnetic field disorder. We observe a similar time evolution for $t \lesssim 10$ under the influence of either potential or field disorder. At larger t and for $W_{c(s)} \leqslant 6$, $P_c(t)$ relaxes towards zero faster in the case of field disorder. At larger $W_{c(s)} \geqslant 10$, $P_c(t)$ shows a slow, logarithmic decrease in time. Provided that the time dependence would further follow a logarithmic form $A\ln(t) + B$, as displayed with thin dashed lines for $W_{c(s)} = 10$ in Fig. 1(a), $P_c(t)$ would equilibrate under W_c or W_s to zero around $\tau_c \sim 27\,000$ and $\tau_s \sim 460\,000$, respectively. It is worth stressing that relaxation time becomes longer in the case of potential disorder at larger values of $W_{c(s)} \geqslant 10$; moreover, relaxation might be prevented by the onset of the many-body localization.

In the case of the spin imbalance $P_s(t)$ [see Fig. 1(b)], we find exceedingly different time evolutions when comparing systems with potential and field disorders. While $P_s(t)$ in the case of the field disorder shows behavior qualitatively similar to that of $P_c(t)$, the time evolution in the case of the potential disorder shows relaxation for all W_s on a timescale accessible by our calculations. Moreover, the corresponding relaxation times τ show a quadratic W_c dependence, as shown in the inset of Fig. 1(b). The latter quadratic dependence may be explained by recalling that for large W_c, ($W_s = 0$) a redistribution of charge may be energetically very costly; however, reversing the spin orientation does not change the energy. Therefore, the charge redistribution that is necessary for the spin dynamics is realized via virtual processes shown in Fig. 1(c). In order to estimate the relevant energy scale (i.e., also the timescale) one may study a toy model with the four local states shown in Fig. 1(c): two initial states $|\uparrow, 0, \downarrow\rangle^{S/A}$ and two virtually generated states $|\uparrow, \downarrow, 0\rangle^{S/A}$. The corresponding eigenproblem is, up to a constant-energy shift, given by 2×2 matrices,

$$\begin{pmatrix} 0 & -t_0 \\ -t_0 & V^{S/A} \end{pmatrix} \begin{pmatrix} |\uparrow, 0, \downarrow\rangle^{S/A} \\ |\uparrow, \downarrow, 0\rangle^{S/A} \end{pmatrix} = E^{S/A} \begin{pmatrix} |\uparrow, 0, \downarrow\rangle^{S/A} \\ |\uparrow, \downarrow, 0\rangle^{S/A} \end{pmatrix}, \quad (6)$$

where the potentials $V^{S/A} = \epsilon_2 - \epsilon_3 - \frac{1}{2}(J_z \mp J_\perp)$. If the charge disorder is strong, then the typical values of $|V^{S/A}| \sim$

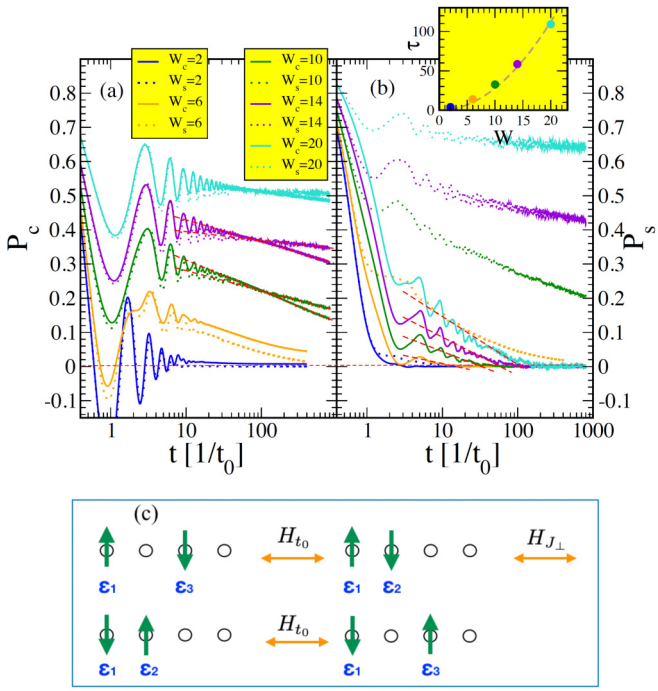

FIG. 1. (a) and (b) $P_{c(s)}(t) = \langle \hat{P}_{c(s)} \rangle_t$ for a system with $L = 16$. Note that $P_{s(c)}(t = 0) = 1$. Results using finite potential disorder W_c (and $W_s = 0$) are presented with solid lines, while those with field disorder W_s (and $W_c = 0$) are presented with dotted lines. Roughly $N_r \sim 500$ realizations have been used for each set of data. The inset in (b) represents the relaxation time τ defined through intercepts of P_s with zero obtained by fitting $P_s(t) = A \ln(t) + B$ in the interval $t \gtrsim 4$ and $t \sim \tau_{\text{approx}}$. Fits are displayed by thin dashed red lines. The brown dashed line in the inset represents the single-parameter fit $\tau = 0.28 W_c^2$. Fits similar to those for $P_s(t)$ in a different time interval for $P_c(t)$ are also displayed in (a) using thin dashed red lines. Relaxation times for $W_{c(s)} = 14$ based on the presented fits are $\tau_c = 4.7 \times 10^6$ and $\tau_s = 7.7 \times 10^{16}$. A small time step $\Delta t = 0.01$ was used in all presented results to obtain sufficient numerical stability of time propagation. (c) Processes that connect two spin-reversed states with equal energy. Here, H_{t_0} and $H_\perp$ represent the first and third terms in Eq. (1) for potential disorder.

$|\epsilon_2 - \epsilon_3|$ are large. As a consequence only two eigenstates have large projections on the initial states, $|\uparrow, 0, \downarrow\rangle^{S/A}$. Then, the dynamics of odd operators is governed by the difference in corresponding eigenenergies in symmetric and antisymmetric sectors $\tau = |E^S - E^A|^{-1} \sim W_c^2 / t_0^2 J_\perp$.

IV. CHARGE AND SPIN CORRELATION FUNCTIONS

We next explore the neighboring density-density and spin-spin correlation functions, defined as

$$\hat{G}_n = \frac{1}{L} \sum_i n_i n_{i+1}, \qquad G_n(t) = \langle \hat{G}_n \rangle_t, \tag{7}$$

$$\hat{G}_{S^z} = \frac{1}{L} \sum_i S_i^z S_{i+1}^z, \qquad G_{S^z}(t) = \langle \hat{G}_{S^z} \rangle_t. \tag{8}$$

For proper analysis of the long-time behavior it is important to note that the energy of the initial state after averaging over different random realizations, $E_{\text{ave}} = \langle \psi_0 | H | \psi_0 \rangle_{\text{ave}} = 0$,

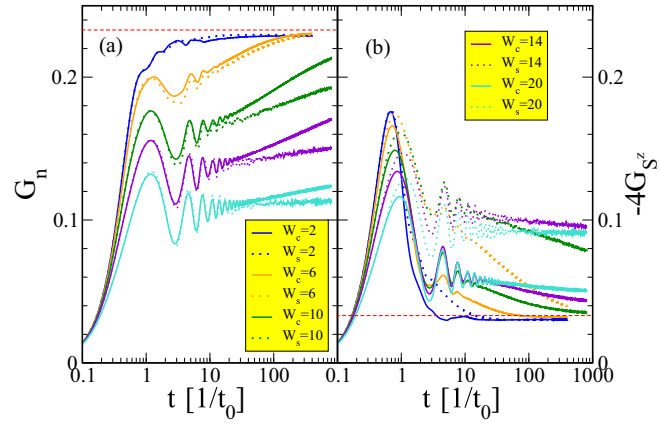

FIG. 2. (a) $G_n(t)$ and (b) $G_{S^z}(t)$ for different strengths of disorder. Solid lines represent potential disorder W_c, while dotted lines show magnetic field disorder W_s. Thin horizontal red dashed lines represent the infinite-T limits of correlation functions, $G_n(T \to \infty) = 7/30$, $G_{S^z}(T \to \infty) = -1/120$. Note that their respective values in the thermodynamic limit are $1/4$ and 0, respectively. The parameters of the system are the same as in Fig. 1.

is located near the middle of the energy spectrum, which in the microcanonical sense corresponds to infinite temperature ($T \to \infty$). Based on the eigenstate thermalization hypothesis [48–54], it is expected that for small $W_{c(s)}$ and $t \to \infty$, $G_{n(S^z)}$ approach their respective $T \to \infty$ limits, as indicated by dashed horizontal lines in Fig. 2. It is indicative that charge and spin correlation functions for short times $t \lesssim 1$ display qualitatively similar time dependences. Initially, only the hopping part (the first term) of the Hamiltonian in Eq. (1) is active since the exchange interaction can act only between particles on neighboring sites. The change in either the potential energy or field energy after hopping between neighboring lattice sites is in both cases comparable, which leads to a similar time dependence for times comparable to the inverse hopping time $1/t_0$. For larger $W_{c(s)} \gtrsim 10$ and $t \gtrsim 50$, G_n shows a logarithmic increase in time, while G_{S^z} shows a logarithmic decrease. The difference is due to substantially different $T \to \infty$ limits. In contrast to G_n, G_{S^z} shows distinct dependence with regard to the type of disorder. At large $W_c \geqslant 10$, G_{S^z} approaches significantly closer to the ergodic $T \to \infty$ limit than in the case of $W_s \geqslant 10$. Still, G_{S^z} does not show relaxation, which is the case of $P_s(t)$, shown in Fig. 1(b). The explanation for this seeming discrepancy can be found again in the symmetry argument. While $\hat{P}_s$ is odd under the $\mathbb{Z}_2$ spin transformation, $\hat{G}_{S^z}$ is even, it has nonzero matrix elements within a fixed symmetry sector, and the matrix elements which are diagonal in the eigenstates of Hamiltonian may be nonzero as well.

To test this assumption, we define a three-site operator,

$$\hat{\Gamma} = \frac{8}{N_f} \sum_{i=1,3,5,\ldots,L-1} (-1)^{1+(i+1)/2} S_i^z S_{i+2}^z S_{i+4}^z, \tag{9}$$

which is also odd under the $\mathbb{Z}_2$ spin transformation, $\hat{U} \hat{\Gamma} \hat{U} = -\hat{\Gamma}$. As seen in Fig. 3, $\Gamma(t) = \langle \hat{\Gamma} \rangle_t$ also shows relaxation with the respective relaxation times τ_Γ scaling with W_c^2 just as in the case of $P_c(t)$, shown in Fig. 1(b).

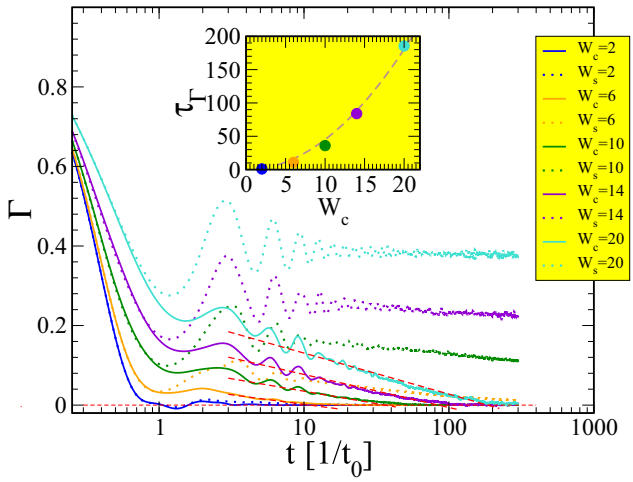

FIG. 3. $\Gamma(t) = \langle \hat{\Gamma} \rangle_t$ for different strengths of disorder. Solid lines represent potential disorder W_c, while dotted lines show magnetic field disorder W_s. Dashed red lines represent fits of the form $\Gamma(t) = A \ln(t) + B$ that were used to extract relaxation times τ_Γ, presented in the inset. The dashed brown line in the inset represents the single-parameter fit $\tau_\Gamma = 0.45 W_c^2$. The parameters of the system are the same as in Fig. 1.

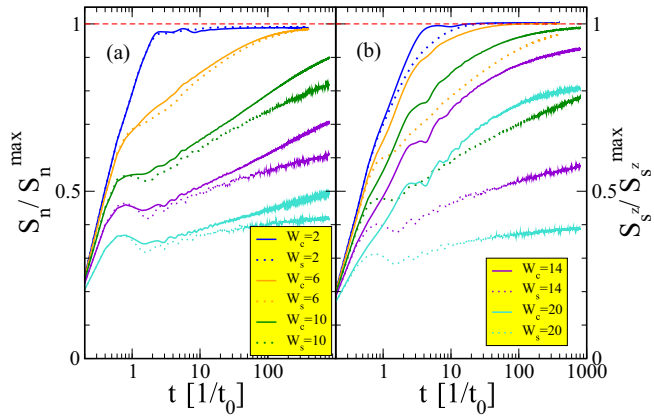

FIG. 4. (a) $S_n(t)$ and (b) $S_{S^z}(t)$ for different strengths of disorder. Solid lines represent potential disorder W_c, while dotted lines show magnetic field disorder W_s. Results are normalized to their respective values in the infinite-T limit, $S_n^{\max} \sim 1.45$ and $S_{S^z}^{\max} \sim 1.80$. The parameters of the system are the same as in Fig. 1.

V. SPIN AND CHARGE ENTANGLEMENT ENTROPY

We now turn to a comparison of the dynamics of the entanglement properties of charge and spin degrees of freedom. To this end we split the system into two halves. We then compute the charge and spin entanglement entropies [19,55], respectively,

$$S_n = -\sum_{n=0}^{N_f} p_n \ln(p_n), \tag{10}$$

$$S_{S^z} = -\sum_{S^z=-S^z_{\max}}^{S^z_{\max}} p_{S^z} \ln(p_{S^z}), \tag{11}$$

where $S^z_{\max} = N_f/4$ and p_n and p_{S^z} represent the probabilities that the subsystem contains n fermions and the z component of the total spin equals S^z, respectively.

The charge entropy S_n, shown in Fig. 4(a), displays qualitatively similar behavior with respect to the potential and field disorders for small $W_{c(s)} \leqslant 6$. In both cases S_n approaches its maximal value, characteristic of a thermal state at $t \to \infty$. For larger $W_{c(s)} \geqslant 10$ we observe a stronger deviation for different types of disorder in the long-time limit. In both cases we observe a slow logarithmic increase, characteristic of MBL systems.

In contrast, the spin entropy S_{S^z} quantitatively differs in comparison to potential or field disorder in the whole range of $W_{c(s)}$. The most significant difference is observed when comparing results for larger $W_{c(s)} \geqslant 10$, where $S_{S^z}(W_c)$ grows significantly faster than $S_{S^z}(W_s)$. For example, while at $W_{c(s)} = 10$, $S_{S^z}(W_c)$ nearly reaches its maximal value $S_{S^z}^{\max}$, $S_{S^z}(W_s)$ displays slow logarithmic growth. For even larger $W_c \geqslant 14$ there seems to be no observable time interval with logarithmic growth of $S_{S^z}(W_c)$. In contrast, it shows a tendency towards saturation towards a nonthermal value.

To gain a deeper physical picture we first note that while the field disorder affects charge as well as spin degrees of freedom, the potential disorder affects only charge degrees of freedom. For example, when a fermion with spin up hops between neighboring sites under the influence of field disorder, it feels different Zeeman energy just like when in the presence of the potential disorder it feels different potential energy. Connected spin chains separated by empty sites exist. Spins that form a particular connected spin chain do not feel the potential disorder as long as they remain attached to the chain. Spin excitation can freely propagate along a connected spin chain in the presence of the potential disorder. When such connected spin chains extend between the boundaries of the two subsystems, they contribute to the growth of spin entropy.

VI. SPECTRAL LEVEL STATISTICS

Motivated by the rather unexpected difference in the time evolution of charge vs spin imbalance, observed in Fig. 1(b), as well as other observables probing charge or spin degrees of freedom under the influence of potential disorder, we next explore the statistical properties of the energy spectra. We compute adjacent energy level spacing ratios $r_n = \min[\Delta_n, \Delta_{n-1}]/\max[\Delta_n, \Delta_{n-1}]$, where $\Delta_n = E_n - E_{n-1}$ and $\{E_n\}$ represents the ordered set of energy levels of the Hamiltonian in Eq. (1). For each realization of disorder we compute the average value of $\bar{r}$ and then instead of computing the average over different realizations, we calculate the cumulative distribution function for $\bar{r}$, $F(\bar{r})$. In Fig. 5(a) we first present $F(\bar{r})$ for the case of potential disorder W_c, taking into account the full spectrum. Since the Hamiltonian in Eq. (1) is nonintegrable, one expects that at small $W_c = 2$ its spectrum resembles the spectrum of the Gaussian random matrices where $\bar{r}_{\text{ave}} = \bar{r}_{\text{GOE}} \simeq 0.53$ [3,56]. In contrast, at large $W_c = 20$, the average value of $\bar{r}$ should not drop below $r_{\text{Poisson}} = 0.386$, characteristic of a random distribution of energy levels. Distributions $F(\bar{r})$, shown in Fig. 5(a), are not consistent with either of the above predictions.

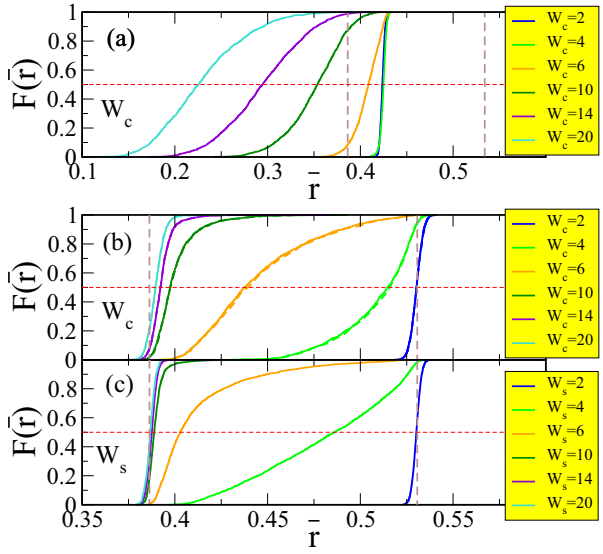

FIG. 5. $F(\bar{r})$ for different values of potential disorder (a) from the full spectrum and (b) from the symmetric (solid lines) and the antisymmetric (dashed lines) parts of the spectra and (c) for field disorder. Vertical dashes lines indicate values of $r_{\text{Poisson}} \simeq 0.386$ and $r_{\text{GOE}} \simeq 0.53$. In most cases $N_r \sim 1500$ samples have been used. Results were obtain using full diagonalization on a system with $L = 12$, $N_\uparrow = N_\downarrow = 3$, and $N_{\text{states}} = 18480$.

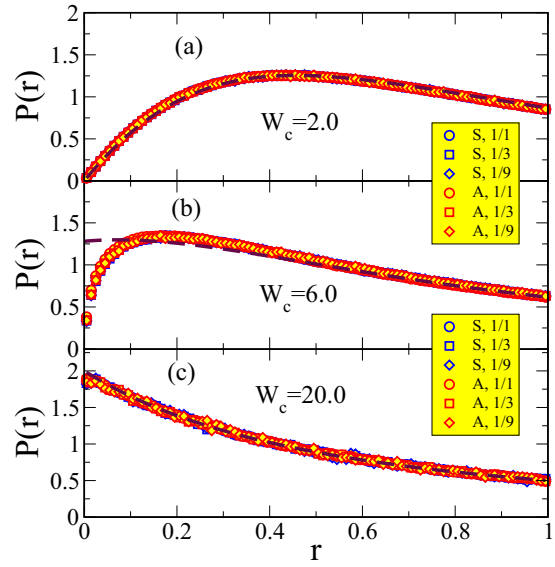

FIG. 6. Points show the probability density of the gap ratio for charge disorder obtained from the symmetric (S) and antisymmetric (A) parts of the spectra. The fractions in the legend mark the parts of the spectra which were used to generate the distribution. The dashed lines in (a) and (c) show Eqs. (13) and (12), respectively. The dashed line in (b) shows the distribution given by Eq. (20) in Ref. [59] with a normalization that is relevant for $r \in (0, 1)$.

For a proper analysis of the spectral level statistics in the case of the potential disorder we have computed $F(\bar{r})$ separately for each symmetry subspace. In Figs. 5(b) and 5(c) we present $F(\bar{r})$ for different values of $W_{c(s)}$. There are two types of nearly overlapping curves (solid and dashed lines) in the case of potential disorder; see Fig. 5(b), which represents $F(\bar{r})$ for each symmetry sector separately. For small $W_{c(s)} = 2$, presented in Figs. 5(b) and 5(c), $F(\bar{r})$ can be fitted with the error function positioned at $\bar{r}_{\text{ave}} = 0.53$, which agrees with r_{GOE}. At large $W_{c(s)} = 20$, $F(\bar{r})$ again resemble error functions, but in this regime close to r_{Poisson}, which in a finite system indicates localization. For the intermediate values of $W_{c(s)} \in [4, 6]$ we observe broad distributions $F(\bar{r})$ that result from a mixture of systems in which some of them exhibit level statistics that resembles ergodic systems while others are closer to being nonergodic/localized.

We have also calculated the distribution of the gap ratios without averaging r_n over multiple energy levels. To this end we have generated a set containing r_n for various n as well as for various disorder realizations and calculated the probability density $P(r)$ from the histogram of $\{r_n\}$. While the distribution $F(\bar{r})$ in Fig. 5 contains information about differences between various realizations of disorder, such information is not directly encoded in $P(r)$. Nevertheless, $P(r)$ allows for a more detailed comparison with the random matrix theory. For the Poisson level statistics one gets [3]

$$P_P(r) = \frac{2}{(1+r)^2}, \tag{12}$$

while an approximate distribution for the Gaussian orthogonal ensemble (GOE) can be derived from the Wigner surmise [57–59] for three energy levels,

$$P_{\text{GOE}}(r) = \frac{27}{4}\frac{r + r^2}{(1 + r + r^2)^{5/2}}. \tag{13}$$

Figure 6 shows the distributions $P(r)$ obtained from the symmetric (S) and antisymmetric (A) parts of the spectra with charge disorder. In order to identify artifacts arising from the presence of the localization edge, the distributions have been generated either from all levels or from only a central part (1/3 or 1/9) of the levels in the middle of the spectrum. Results obtained for all three cases accurately overlap (see Figs. 6 and 7), indicating the absence of artifacts originating from the localization edge.

As expected, numerical results for weak disorder [Fig. 6(a)] accurately reproduce Eq. (13), whereas for the strong disorder shown in Fig. 6(c), the distribution agrees with Eq. (12). In the vicinity of the transition, $P(r)$ can be well approximated by the mixed Wigner surmise discussed very recently in Ref. [59]. More precisely, the dashed curve in Fig. 6(b) shows the distribution for 2×2 GOE matrices mixed with two uncorrelated energy levels (see Eq. (20) in Ref. [59]). Such a mixture of GOE and Poisson distributions may be interpreted as the coexistence of localized (insulating) and delocalized (metallic) domains in which the absence of level crossings, $F(r \to 0) = 0$ in Fig. 6(b), indicates that localization within the former domains is not perfect. Similar results concerning the spatial separation of conducting and insulating domains were recently found for the random-field Heisenberg model [60].

Figure 7 shows the distribution of the gap ratios obtained for charge disorder from the full spectrum that includes both symmetric and antisymmetric levels. Results obtained for

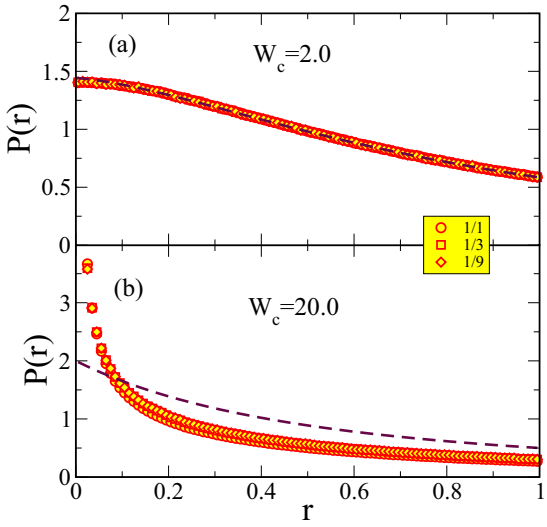

FIG. 7. The same as in Fig. 6, but for a full spectra containing symmetric and antisymmetric levels. The dashed line in (a) shows the distribution given by Eq. (24) in Ref. [59] with a normalization that is relevant for $r \in (0, 1)$, whereas the dashed line in (b) shows Eq. (12).

weak disorder can be very accurately approximated by two independent GOE ensembles. In particular, the dashed dark red line in Fig. 7(a) shows the distribution derived for a mixture of two 2×2 GOE matrices (see Eq. (24) in Ref. [59]). Rather unexpected is the case of strong disorder when $P(r)$ for $r \ll 1$ significantly exceeds the distribution derived for the Poisson statics, as shown in Fig. 7(b). Comparing Figs. 6(c) and 7(b) we identify an attraction between symmetric and antisymmetric energy levels. Such a scenario is consistent with results for the average ratio shown in Fig. 5(a).

VII. SUMMARY

We have studied spin and charge dynamics in a disordered chain such that an unperturbed system has $\mathbb{Z}_2$ spin symmetry. Then we considered two types of disorder: a random magnetic field that breaks the $\mathbb{Z}_2$ symmetry and random charge potential, which preserves the spin symmetry. In the former case with broken spin symmetry, the dynamics of all studied observable are consistent with localization on finite lattices in that their expectation values do not approach the results for thermal equilibrium. However, for the symmetry-preserving disorder, the observables that are odd under the $\mathbb{Z}_2$ spin transformation seem to thermalize while even observables do not. Numerical studies of the time evolution for the symmetry-preserving disorder were accompanied by the level statistics. Interestingly, the level statistics obtained separately for odd and even symmetry sectors accurately reproduce a crossover/transition from the GOE for weak charge disorder to the Poisson distribution for the strong disorder. The time evolution and the level statistics suggest that localization exists within each symmetry sector, i.e., for odd or even eigenstates and observables with matrix elements only within a given symmetry sector. The apparent relaxation of odd operators is not inconsistent with the level statistics since such operators evolve between the two sectors. Similar numerical results were found for the dynamics in the Hubbard model with charge disorder, which, however, has SU(2) symmetry [33–35,61,62]. In the latter model, the spin imbalance decays subdiffusively [33,34,61], while the spin energy density seems not to thermalize [35,62]. In our studies, we have not considered the stability of the localized phase in the thermodynamic limit, so we do not exclude that localization represents extremely slow dynamics that eventually may lead to a thermal equilibrium of an infinite chain.

Comparison of the entanglement entropies of spin and charge degrees of freedom revealed an essential difference between the field disorder that affects charge and spin degrees of freedom and the potential disorder that influences only charge degrees of freedom. Spins that form a particular connected spin chain do not feel potential disorder. Spin excitations can thus freely propagate along a connected spin chain. This may explain the absence of logarithmic growth of the spin entanglement entropy even in the regime of strong potential disorder, where in contrast, the charge entanglement entropy displays logarithmic time evolution.

The original motivation for this work stems from experiments on cold atoms [63] in which charge imbalance was measured in a cold-atom experiment setup. Recent advances in spin- and density-resolved microscopy [64–66] might allow measurements of the charge and spin imbalance under the non-symmetry-breaking disorder.

ACKNOWLEDGMENTS

We acknowledge the support from the National Science Centre, Poland, via Project NO. 2020/37/B/ST3/00020 (M.M.), the support from the Slovenian Research Agency (ARRS), Research Core Funding Grant No. P1-0044 (J.B.), and the support from the Center for Integrated Nanotechnologies, an Office of Science User Facility operated for the U.S. Department of Energy (DOE) Office of Science by Los Alamos National Laboratory (Contract No. 89233218CNA000001) and Sandia National Laboratories (Contract No. DE-NA-0003525; J.B.).

[1] I. V. Gornyi, A. D. Mirlin, and D. G. Polyakov, Interacting Electrons in Disordered Wires: Anderson Localization and Low-t Transport, Phys. Rev. Lett. **95**, 206603 (2005).

[2] D. Basko, I. Aleiner, and B. Altshuler, Metal-insulator transition in a weakly interacting many-electron system with localized single-particle states, Ann. Phys. (NY) **321**, 1126 (2006).

[3] V. Oganesyan and D. A. Huse, Localization of interacting fermions at high temperature, Phys. Rev. B **75**, 155111 (2007).

[4] D. A. Abanin, E. Altman, I. Bloch, and M. Serbyn, Colloquium: Many-body localization, thermalization, and entanglement, Rev. Mod. Phys. **91**, 021001 (2019).

[5] O. S. Barišić and P. Prelovšek, Conductivity in a disordered one-dimensional system of interacting fermions, Phys. Rev. B **82**, 161106(R) (2010).

[6] D. J. Luitz, N. Laflorencie, and F. Alet, Many-body localization edge in the random-field Heisenberg chain, Phys. Rev. B **91**, 081103(R) (2015).

[7] D. J. Luitz, N. Laflorencie, and F. Alet, Extended slow dynamical regime prefiguring the many-body localization transition, Phys. Rev. B **93**, 060201(R) (2016).

[8] E. J. Torres-Herrera and L. F. Santos, Dynamics at the many-body localization transition, Phys. Rev. B **92**, 014208 (2015).

[9] F. Andraschko, T. Enss, and J. Sirker, Purification and Many-Body Localization in Cold Atomic Gases, Phys. Rev. Lett. **113**, 217201 (2014).

[10] A. Pal and D. A. Huse, Many-body localization phase transition, Phys. Rev. B **82**, 174411 (2010).

[11] S. Bera, H. Schomerus, F. Heidrich-Meisner, and J. H. Bardarson, Many-Body Localization Characterized from a One-Particle Perspective, Phys. Rev. Lett. **115**, 046603 (2015).

[12] J. Hauschild, F. Heidrich-Meisner, and F. Pollmann, Domain-wall melting as a probe of many-body localization, Phys. Rev. B **94**, 161109(R) (2016).

[13] T. Devakul and R. R. P. Singh, Early Breakdown of Area-Law Entanglement at the Many-Body Delocalization Transition, Phys. Rev. Lett. **115**, 187201 (2015).

[14] C. L. Bertrand and A. M. García-García, Anomalous Thouless energy and critical statistics on the metallic side of the many-body localization transition, Phys. Rev. B **94**, 144201 (2016).

[15] V. Khemani, S. P. Lim, D. N. Sheng, and D. A. Huse, Critical Properties of the Many-Body Localization Transition, Phys. Rev. X **7**, 021013 (2017).

[16] E. V. H. Doggen, F. Schindler, K. S. Tikhonov, A. D. Mirlin, T. Neupert, D. G. Polyakov, and I. V. Gornyi, Many-body localization and delocalization in large quantum chains, Phys. Rev. B **98**, 174202 (2018).

[17] J. Šuntajs, J. Bonča, T. Prosen, and L. Vidmar, Quantum chaos challenges many-body localization, Phys. Rev. E **102**, 062144 (2020).

[18] J. Šuntajs, J. Bonča, T. Prosen, and L. Vidmar, Ergodicity breaking transition in finite disordered spin chains, Phys. Rev. B **102**, 064207 (2020).

[19] M. Kiefer-Emmanouilidis, R. Unanyan, M. Fleischhauer, and J. Sirker, Evidence for Unbounded Growth of the Number Entropy in Many-Body Localized Phases, Phys. Rev. Lett. **124**, 243601 (2020).

[20] D. J. Luitz and Y. B. Lev, Absence of slow particle transport in the many-body localized phase, Phys. Rev. B **102**, 100202(R) (2020).

[21] D. Abanin, J. Bardarson, G. De Tomasi, S. Gopalakrishnan, V. Khemani, S. Parameswaran, F. Pollmann, A. Potter, M. Serbyn, and R. Vasseur, Distinguishing localization from chaos: Challenges in finite-size systems, Ann. Phys. (NY) **427**, 168415 (2021).

[22] D. Sels and A. Polkovnikov, Dynamical obstruction to localization in a disordered spin chain, Phys. Rev. E **104**, 054105 (2021).

[23] P. Sierant, E. G. Lazo, M. Dalmonte, A. Scardicchio, and J. Zakrzewski, Constraint-Induced Delocalization, Phys. Rev. Lett. **127**, 126603 (2021).

[24] L. Vidmar, B. Krajewski, J. Bonča, and M. Mierzejewski, Phenomenology of Spectral Functions in Disordered Spin Chains at Infinite Temperature, Phys. Rev. Lett. **127**, 230603 (2021).

[25] A. Morningstar, L. Colmenarez, V. Khemani, D. J. Luitz, and D. A. Huse, Avalanches and many-body resonances in many-body localized systems, arXiv:2107.05642.

[26] D. Sels, Markovian baths and quantum avalanches, arXiv:2108.10796.

[27] M. Kiefer-Emmanouilidis, R. Unanyan, M. Fleischhauer, and J. Sirker, Unlimited growth of particle fluctuations in many-body localized phases, Ann. Phys. (NY) **435**, 168481 (2021).

[28] A. C. Potter and R. Vasseur, Symmetry constraints on many-body localization, Phys. Rev. B **94**, 224206 (2016).

[29] A. Chandran, V. Khemani, C. R. Laumann, and S. L. Sondhi, Many-body localization and symmetry-protected topological order, Phys. Rev. B **89**, 144201 (2014).

[30] I. V. Protopopov, W. W. Ho, and D. A. Abanin, Effect of SU(2) symmetry on many-body localization and thermalization, Phys. Rev. B **96**, 041122(R) (2017).

[31] B. Ware, D. Abanin, and R. Vasseur, Perturbative instability of nonergodic phases in non-Abelian quantum chains, Phys. Rev. B **103**, 094203 (2021).

[32] A. J. Friedman, R. Vasseur, A. C. Potter, and S. A. Parameswaran, Localization-protected order in spin chains with non-Abelian discrete symmetries, Phys. Rev. B **98**, 064203 (2018).

[33] P. Prelovšek, O. S. Barišić, and M. Žnidarič, Absence of full many-body localization in the disordered Hubbard chain, Phys. Rev. B **94**, 241104(R) (2016).

[34] M. Sroda, P. Prelovšek, and M. Mierzejewski, Instability of sub-diffusive spin dynamics in strongly disordered Hubbard chain, Phys. Rev. B **99**, 121110(R) (2019).

[35] M. Kozarzewski, M. Mierzejewski, and P. Prelovšek, Suppressed energy transport in the strongly disordered Hubbard chain, Phys. Rev. B **99**, 241113(R) (2019).

[36] I. V. Protopopov and D. A. Abanin, Spin-mediated particle transport in the disordered Hubbard model, Phys. Rev. B **99**, 115111(R) (2019).

[37] R. Mondaini and M. Rigol, Many-body localization and thermalization in disordered Hubbard chains, Phys. Rev. A **92**, 041601(R) (2015).

[38] M. Mierzejewski, M. Kozarzewski, and P. Prelovšek, Counting local integrals of motion in disordered spinless-fermion and Hubbard chains, Phys. Rev. B **97**, 064204 (2018).

[39] J. Bonča and M. Mierzejewski, Delocalized carriers in the t-J model with strong charge disorder, Phys. Rev. B **95**, 214201 (2017).

[40] F. J. Dyson, The dynamics of a disordered linear chain, Phys. Rev. **92**, 1331 (1953).

[41] G. Theodorou and M. H. Cohen, Extended states in a one-dimensional system with off-diagonal disorder, Phys. Rev. B **13**, 4597 (1976).

[42] T. P. Eggarter and R. Riedinger, Singular behavior of tight-binding chains with off-diagonal disorder, Phys. Rev. B **18**, 569 (1978).

[43] P. W. Brouwer, C. Mudry, B. D. Simons, and A. Altland, Delocalization in Coupled One-Dimensional Chains, Phys. Rev. Lett. **81**, 862 (1998).

[44] P. Brouwer, C. Mudry, and A. Furusaki, Nonuniversality in quantum wires with off-diagonal disorder: A geometric point of view, Nucl. Phys. B **565**, 653 (2000).

[45] C. Mudry, P. W. Brouwer, and A. Furusaki, Crossover from the chiral to the standard universality classes in the conductance of a quantum wire with random hopping only, Phys. Rev. B **62**, 8249 (2000).

[46] F. Evers and A. D. Mirlin, Anderson transitions, Rev. Mod. Phys. **80**, 1355 (2008).

[47] K. Joel, D. Kollmar, and L. F. Santos, An introduction to the spectrum, symmetries, and dynamics of spin-1/2 Heisenberg chains, Am. J. Phys. **81**, 450 (2013).

[48] M. Srednicki, Chaos and quantum thermalization, Phys. Rev. E **50**, 888 (1994).

[49] M. Rigol, V. Dunjko, and M. Olshanii, Thermalization and its mechanism for generic isolated quantum systems, Nature (London) **452**, 854 (2008).

[50] J. M. Deutsch, Quantum statistical mechanics in a closed system, Phys. Rev. A **43**, 2046 (1991).

[51] L. D'Alessio, Y. Kafri, A. Polkovnikov, and M. Rigol, From quantum chaos and eigenstate thermalization to statistical mechanics and thermodynamics, Adv. Phys. **65**, 239 (2016).

[52] J. Eisert, M. Friesdorf, and C. Gogolin, Quantum many-body systems out of equilibrium, Nat. Phys. **11**, 124 (2015).

[53] J. M. Deutsch, Eigenstate thermalization hypothesis, Rep. Prog. Phys. **81**, 082001 (2018).

[54] T. Mori, T. N. Ikeda, E. Kaminishi, and M. Ueda, Thermalization and prethermalization in isolated quantum systems: A theoretical overview, J. Phys. B **51**, 112001 (2018).

[55] A. Lukin, M. Rispoli, R. Schittko, M. E. Tai, A. M. Kaufman, S. Choi, V. Khemani, J. Léonard, and M. Greiner, Probing entanglement in a many-body–localized system, Science **364**, 256 (2019).

[56] S. Mukerjee, V. Oganesyan, and D. Huse, Statistical theory of transport by strongly interacting lattice fermions, Phys. Rev. B **73**, 035113 (2006).

[57] Y. Y. Atas, E. Bogomolny, O. Giraud, and G. Roux, Distribution of the Ratio of Consecutive Level Spacings in Random Matrix Ensembles, Phys. Rev. Lett. **110**, 084101 (2013).

[58] O. Giraud, N. Macé, E. Vernier, and F. Alet, Probing Symmetries of Quantum Many-Body Systems through Gap Ratio Statistics, Phys. Rev. X **12**, 011006 (2022).

[59] M. Fremling, Exact gap-ratio results for mixed Wigner surmises of up to 4 eigenvalues, arXiv:2202.01090.

[60] J. Herbrych, M. Mierzejewski, and P. Prelovšek, Relaxation at different length scales in models of many-body localization, Phys. Rev. B **105**, L081105 (2022).

[61] M. Kozarzewski, P. Prelovšek, and M. Mierzejewski, Spin Subdiffusion in the Disordered Hubbard Chain, Phys. Rev. Lett. **120**, 246602 (2018).

[62] I. V. Protopopov, R. K. Panda, T. Parolini, A. Scardicchio, E. Demler, and D. A. Abanin, Non-Abelian Symmetries and Disorder: A Broad Nonergodic Regime and Anomalous Thermalization, Phys. Rev. X **10**, 011025 (2020).

[63] M. Schreiber, S. S. Hodgman, P. Bordia, H. P. Lüschen, M. H. Fischer, R. Vosk, E. Altman, U. Schneider, and I. Bloch, Observation of many-body localization of interacting fermions in a quasi-random optical lattice, Science **349**, 842 (2015).

[64] M. Boll, T. A. Hilker, G. Salomon, A. Omran, J. Nespolo, L. Pollet, I. Bloch, and C. Gross, Spin- and density-resolved microscopy of antiferromagnetic correlations in fermi-hubbard chains, Science **353**, 1257 (2016).

[65] J. Koepsell, S. Hirthe, D. Bourgund, P. Sompet, J. Vijayan, G. Salomon, C. Gross, and I. Bloch, Robust Bilayer Charge Pumping for Spin- and Density-Resolved Quantum Gas Microscopy, Phys. Rev. Lett. **125**, 010403 (2020).

[66] J. Vijayan, P. Sompet, G. Salomon, J. Koepsell, S. Hirthe, A. Bohrdt, F. Grusdt, I. Bloch, and C. Gross, Time-resolved observation of spin-charge deconfinement in fermionic Hubbard chains, Science **367**, 186 (2020).